

Neural Scaling Laws for Learning-based Identification of Nonlinear Systems

Hannes Gernandt, Marco Roschkowski, Karim Cherifi
University of Wuppertal
`{gernandt, roschkowski, cherifi}@uni-wuppertal.de`

December 24, 2025

Abstract

The use of machine learning models in system identification has increased due to their ability to approximate complex nonlinear dynamics with high accuracy. However, often it is not clear how the performance of trained models scales with given resources such as data, compute, and model size. To allow for a better understanding of the scalability of the performance of machine learning models, we verify neural scaling laws (NSLs) in the context of system identification from input-state-output data using different evaluation metrics for accuracy and different system architectures, including input-affine and physics-informed port-Hamiltonian representations. Our verified NSLs can help to forecast performance improvements and guide model design or data acquisition.

Keywords: System identification, neural scaling laws, port-Hamiltonian systems, nonlinear systems, control applications

1 Introduction

System identification is a discipline in systems and control theory that deals with the building of mathematical models of dynamical systems from data [12]. Classical approaches rely on linear models and carefully designed experiments, which provide strong guarantees and interpretability but often

fall short when dealing with the complex, nonlinear dynamics that appear in many modern engineering and scientific applications.

In recent years, the increasing availability of data and computational power has opened the door to machine learning-based approaches to system identification. Neural networks and other flexible function approximators have shown great promise in capturing complex nonlinear dynamics that are difficult to model with classical methods. Nonlinear system identification is particularly important for modern applications such as robotics, autonomous driving, and climate modeling, where dynamics are inherently complex and linear approximations are often insufficient. Alongside purely data-driven approaches, there has also been a surge of interest in physics-informed learning methods, which aim to integrate domain knowledge and physical priors into the identification process, thereby improving sample efficiency, robustness and interpretability.

Despite these advances, fundamental challenges remain in the identification of nonlinear systems. Training large neural models is computationally expensive, data collection may be costly or time-consuming, and there are no clear rules for determining whether a given identification task is feasible under resource constraints. These bottlenecks motivate the need for neural scaling laws (NSLs), which are predictive rules that relate the accuracy of the model to the amount of data, computation, and model capacity. In machine learning, NSLs have emerged as a powerful tool to guide practitioners in allocating resources for training large models [9].

NSLs were first studied in [9] with the key finding that these typically take the very simple form of a saturated power law

$$L(r) = \alpha + \beta r^\delta \quad (1)$$

with $\alpha, \beta \geq 0, \delta < 0$. In [9], it was also pointed out that a certain amount of minimal resources must be committed to observe this scaling behavior. With a very small amount of resources, the model will only be able to learn “best guessing”. On the log-log scale, (1) is the graph of a function that is approximately linear with slope δ representing smooth scaling. The scaling then saturates once r is large enough such that $\alpha \sim \beta r^\delta$.

NSLs have been observed for several machine learning tasks such as language models [10] where NSLs have been used to predict the resources necessary to successfully train a 175 billion parameter large language model [5]. In addition, NSLs were determined for image-text models in [1], for vision

transformers in [22], and for language image pretraining [8]. Recently, feature learning has been investigated as a way to improve NSLs in [4]. There have also been theoretical efforts in understanding NSLs [13, 2, 15].

In this paper, we bring these ideas to the domain of system identification. Specifically, we present the first systematic experimental study of NSLs in this context. Our results show how scaling behavior manifests itself in system identification tasks, and we provide practical information on the resources required to achieve the desired accuracy. We believe that these findings offer a principled way to evaluate the feasibility of identification problems and to plan resource allocation.

By training thousands of system identification models, we obtain a large set of outcomes consisting of the evaluation metrics and data size, compute, and model capacity for each of those trained models. This set of outcomes allows us to determine the NSLs of the corresponding combination of dataset and identification method. We observe that NSLs in system identification may have several breaks as laid out by [6] and, therefore, we have adapted the definition of a broken NSL from [6] to the system identification context and study NSLs of the form

$$L(r) = \alpha + \beta r^{\delta_0} \prod_{i=1}^b \left[1 + \left(\frac{r}{\sigma_i} \right)^{\frac{1}{\varphi_i}} \right]^{\delta_i \cdot \varphi_i} \quad (2)$$

for a suitable choice of real parameters $\alpha, \beta, \sigma_i, \varphi_i, \delta_i$ and the number of breaks $b \geq 0$. Note that for $b = 0$ breaks we recover the saturated power law (1).

Our contributions and findings can be summarized as follows:

- We propose a modified definition of NSLs (2) in the context of learning based system identification and verify them for various examples and system architectures
- Early trends in the scaling curve allow us to anticipate the data, compute, and model complexity required for higher accuracy. This can be used to accelerate the systematic development of learning-based system identification methods.
- We show that the amount of data is more important than the model size. A larger model does not necessarily yield better results, as indicated by model NSLs often saturating with relatively few parameters. This is in contrast to results in the natural language processing community; see [5].

- Training of system models for an unexpectedly large number of epochs can still reduce the evaluation error.
- Imposing a physical structure, such as port-Hamiltonian models, does not deteriorate the system identification performance and, in some cases, it is even better.

The rest of the paper is organized as follows. In Section 2, we recall learning-based system identification methods and system architectures that are used in this paper. In Section 3, we define a general class of NSLs that we use in the context of system identification. In Section 4 we present our experimental setup to generate the set of outcomes and describe how the NSLs are approximated from these outcomes. In Section 5, we verify compute, data, and model NSLs for several example systems.

2 Learning-based system identification from input-state-output data

In order to study NSLs in system identification, we consider a family of models that can approximate a broad range of control systems while still allowing for systematic variation in data, model size, and training compute. Specifically, we consider three architectures of control systems ranging from unstructured models to physics-based modeling approach:

- *unstructured* systems without structural restrictions

$$\dot{x}(t) = f(x(t), u(t)), \quad y(t) = g(x(t)), \quad (3a)$$

with state $x(t) \in \mathbb{R}^n$, input $u(t) \in \mathbb{R}^m$, output $y(t) \in \mathbb{R}^l$ and for some $f : \mathbb{R}^n \times \mathbb{R}^m \rightarrow \mathbb{R}^n$ and $g : \mathbb{R}^n \rightarrow \mathbb{R}^l$;

- *input-affine* systems

$$\dot{x}(t) = h(x(t)) + j(x(t))u(t), \quad y(t) = k(x(t)), \quad (3b)$$

where $h : \mathbb{R}^n \rightarrow \mathbb{R}^n$, $k : \mathbb{R}^n \rightarrow \mathbb{R}^l$ and $j : \mathbb{R}^n \rightarrow \mathbb{R}^{n \times m}$;

- *port-Hamiltonian* (pH) systems

$$\begin{aligned} \dot{x}(t) &= (J(x(t)) - R(x(t)))\nabla H(x(t)) + B(x(t))u(t), \\ y(t) &= B(x(t))^\top \nabla H(x(t)), \end{aligned} \quad (3c)$$

with matrix-valued functions $J, R : \mathbb{R}^n \rightarrow \mathbb{R}^{n \times n}$, $B : \mathbb{R}^n \rightarrow \mathbb{R}^{n \times m}$, a continuously differentiable Hamiltonian $H : \mathbb{R}^n \rightarrow [0, \infty)$, with gradient $\nabla H(x) \in \mathbb{R}^n$, and with $J(x) = -J(x)^\top$ and $R(x) = R(x)^\top \geq 0$.

Compared to (3a) and (3b), the structural constraints on the system coefficients in the pH representation (3c) guarantee that the learned model preserves physical properties such as passivity, energy dissipation or energy conservation [18].

Our approach to learning-based system identification is based on neural network parameterizations of dynamical systems where we represent all unknown functions in (3a), (3b) and (3c) by multilayer perceptrons (MLPs) to enable the approximation of general nonlinear dependencies. In pH systems, maintaining the pH structure of the functions in (3c) requires customized parameterizations, as outlined by [7].

In the learning-based system identification, we assume that there is a sufficiently rich collection of input-state-output data that is generated based on [7, 14, 19]. We uniformly sample initial states $x_{i,0} \sim U(x_{i,\min}, x_{i,\max})$, $i = 1, \dots, n$, where the choice of $x_{i,\min}$ and $x_{i,\max}$ depends on the particular application, and we consider input signals

$$u(t) = \sum_{k=1}^N a \sin(2\pi k f_0 t + \phi_k), \quad (3)$$

for suitable parameters $f_0, N, a > 0$ and uniformly random sampled phases $\phi_k \in [0, 2\pi)$.

For the data sets given, the functions of all three architectures (unstructured, input-affine, pH) given by (3a), (3b), and (3c) are approximated by MLPs as explained in [7]. For the training of the MLPs, we use the same MSE-type loss function as in [7], that is normalized over individual batches and we normalize the states and inputs before processing those with the neural networks.

In the following, we collect all generated trajectories for all initial values x_0 and all input functions u and over a certain time horizon with time-step size Δt in matrices $\dot{X} = (\dot{x}_{ij}) \in \mathbb{R}^{K \times n}$ where $K \in \mathbb{N}$ denotes the number of data points. The resulting trajectories that are obtained after training for the same initial values and input functions are denoted by $\hat{\dot{X}} = (\hat{\dot{x}}_{ij}) \in \mathbb{R}^{K \times n}$.

We consider the evaluation metrics

$$\text{nMAE}(\dot{X}, \hat{X}) = \frac{1}{K} \sum_{i=1}^K \sum_{j=1}^n \frac{|\dot{x}_{ij} - \hat{\dot{x}}_{ij}|}{\sigma_j}, \quad (4)$$

$$\text{nMSE}(\dot{X}, \hat{X}) = \frac{1}{K} \sum_{i=1}^K \sum_{j=1}^n \left(\frac{\dot{x}_{ij} - \hat{\dot{x}}_{ij}}{\sigma_j} \right)^2, \quad (5)$$

where σ_j is the standard deviation of the derivative of the j th state on the entire dataset. Note that normalization is necessary because a plain MSE or MAE metric would not equally balance the error on all states if these have different magnitudes.

3 Neural scaling laws for system identification

NSLs quantify the intuitive dependence between the model validation error given by the nMAE metric (4) or the nMSE metric (5) and the used *resources* $r > 0$, where r represents either the *size of the dataset* d , the *model parameters* p , or the *compute used during training* c in flops.

We will now give a definition of NSL that is tailored to our application to system identification. To derive NSL we select one of the resources r (data, compute or model size) and vary over this resource and the remaining training parameters. For the resource r and each such parameter configuration, we perform a training run for the model and compute the validation error e of the learned model based on (4) or (5). By repeating the training runs for different resources r_i and collecting the resulting validation errors e_i leads to a set of *outcomes* $O = \{(r_1, e_1), (r_2, e_2), \dots, (r_J, e_J)\}$ in \mathbb{R}_+^2 . Note that in the set of outcomes we neglect the dependence on the other training parameters. For example, if the resource r represents the size of the data set, then two points (r_i, e_i) and (r_j, e_j) which are close in \mathbb{R}^2 can result from quite different computing resources and model sizes.

For the approximation of NSL, we assume that without restriction the entries of O are ordered with respect to the size of the resources, i.e. $r_1 \leq r_2 \leq \dots \leq r_J$ and we define the *lower envelope* $E : [r_1, r_J] \rightarrow [0, \infty)$ given by

$$E(r) := \min\{e_i \mid i = 1, \dots, J, r_i \leq r\}. \quad (6)$$

Furthermore, we generate additional interpolation points by choosing a grid size $K \in \mathbb{N}$ and

$$r_0 = \tilde{r}_0 \leq \tilde{r}_1 \leq \cdots \leq \tilde{r}_K = r_J, \quad \tilde{r}_k := r_0^{1-\frac{k}{K}} r_J^{\frac{k}{K}}. \quad (7)$$

Since the resources r_i typically vary at exponential scale, the choice of the interpolation points $\{\tilde{r}_i\}_{i=1}^K$ achieves an equidistant partitioning on log-scale. Furthermore, for each interpolation point, we set $\tilde{e}_k = E(\tilde{r}_k)$.

Definition 3.1. Consider a set of outcomes $O \subseteq \mathbb{R}_+^2$, lower envelope E defined as (6) and interpolation points $\{\tilde{r}_i\}_{i=1}^K$ given by (7). Then O obeys a *NSL with at most b breaks and margin $M > 0$* if there are $\alpha, \beta \geq 0 \geq \delta_i$ and $\sigma_i, \varphi_i > 0$, $b \in \mathbb{N}_0$ such that the function $L : [r_1, r_J] \rightarrow \mathbb{R}$ given by

$$L(r) = \alpha + \beta r^{\delta_0} \prod_{i=1}^b \left[1 + \left(\frac{r}{\sigma_i} \right)^{\frac{1}{\varphi_i}} \right]^{\delta_i \cdot \varphi_i} \quad (8)$$

satisfies

$$M = \frac{1}{K} \sum_{k=1}^K (\log \hat{e}_k - \log \tilde{e}_k)^2 \quad (9)$$

with $\hat{e}_k = L(\tilde{r}_k)$ and $\tilde{e}_k = E(\tilde{r}_k)$. \square

Compared to existing definitions for NSLs in the literature, we use a broken scaling law [6] and quantify in Definition 3.1 an approximation margin M of the NSL which is particularly motivated by the applications to system identification. In this context, NSL have to be verified for different architectures (3a), (3b), (3c), various datasets for different application examples and the different resource types data, compute, and model parameters. Here, Definition 3.1 allows us to (semi-) automatically compute the NSL and validate its margin M in a well-defined manner independent of the particular setup. Note that other choices of the lower envelope E are also possible. For example, another possible choice is to interpolate between the nearest points. However, for our datasets this does not make a huge difference since there is typically only a small gap between e_i and e_{i+1} . We also point out that equally spacing the e_i at log-scale is necessary for (9) to be meaningful. Indeed if we would have simply used all the points in O , the margin would be highly biased towards regions containing a high density of configurations.

4 Generating outcomes and approximation of NSLs

In this section, we explain how the sets of outcomes are generated and how the NSLs were fitted to the observed data relating resources and validation error of a large number of training runs.

4.1 Model training

We train the models on the same nonlinear example systems as in [7]:

- An interconnected mass-spring-damper chain which contains nonlinear dissipation, abbreviated as the *spring system*;
- a magnetically levitated ball system which contains nonlinear dissipation and a nonlinear Hamiltonian, abbreviated as the *ball system*;
- a permanent magnet synchronous motor (PMSM) which contains a nonlinear interconnection matrix $J(x)$, see (3c), abbreviated as the *motor system*.

A detailed description of these systems is given in the appendix.

We vary the number of trajectories, training epochs, depth of the model and hidden dimensions of the model and use the same training script to gather the training evaluations necessary to determine NSLs. The number of epochs used to train the model runs over a grid of $n_e = 2, 4, \dots, 2^{14}$.

One full trajectory represents a 10 seconds long simulation of the system with time discretization $\Delta t = 0.01$ seconds which implies that one trajectory consists of 1000 data points. We first randomly select $\tilde{d} = 2, 4, \dots, 2^9$. We then select a random float $d \in [\tilde{d}/2, \tilde{d}]$. The number of training trajectories is then $n_t = \frac{d}{10}$. Since n_t need not be an integer, we also consider fractional trajectories which are computed by $n_t = 10 \cdot a + b$, $a \in \mathbb{N}$, $b \in [0, 1)$. We then generate $a + 1$ trajectories and use the first a full trajectories. Finally, we select the smallest integer \tilde{b} which is smaller than $b \cdot 1000$ and use the first \tilde{b} data points from the last trajectory. It is important to consider fractional trajectories since the interval $[2^0, 2^1]$ contains very few integers. Hence considering fractional trajectories allows to explore significantly more configurations for small data sizes.

The hidden dimension of the model is obtained by running a loop with values $\tilde{n}_h = 2, 4, 8, 16$ and selecting a random integer n_h between $\tilde{n}_h/2$ and \tilde{n}_h . The reason is again that we want to consider as many model sizes as possible. Similarly, the depth of the model is obtained by running a loop for the depth with values $\tilde{n}_d = 2, 4$ and selecting a random integer n_d between $\tilde{n}_d/2$ and \tilde{n}_d . As in [7], the hidden dimension for the MLP is multiplied by 2 and rounded for unstructured models, to compensate for structured models using more sub-modules, roughly equalizing the parameter count at a given hidden dimension. The total parameter count then equals approximately $4 \cdot n_d \cdot n_h^2$. Finally, all these loops are nested in the lines 4–7 of Pseudo code 1, resulting in the submission of $9 \cdot 14 \cdot 4 \cdot 2 = 1008$ experiments being performed per dataset/architecture combination. We found that there is a failure rate of approximately 3%. Thus, the outcomes of such experiments are not considered.

We use random seeds that determine the random selection of T, n_h and n_d to ensure reproducibility of our experiments and vary the seed to obtain more experiments with different random choices and we use $N = 7$ different random seeds to obtain a large enough set of outcomes. In line 13 of Pseudo code 1, the expression `'main(n_e, n_t, n_d, n_h, A, D)'` is an abbreviation for submitting a job where a model with depth n_d , hidden dimension n_h is trained with the number of training trajectories n_t and number of training epochs n_e on the dataset D with architecture A . We use the general formula $c = p \cdot n_e \cdot n_t \cdot 1000$ to estimate the compute in flops, which follows directly from the fact that each parameter contributes one floating-point operation per sample during the forward pass. This function then returns the metrics nMAE, nMSE and the number of parameters of the model p which is computed in the main script by explicitly counting the parameters occurring in all MLPs that are used to parametrize the system architecture using PyTorch functions. The set of outcomes can then be read out from the logs which are managed using *mlflow* [21].

The total number of jobs submitted this way amounts to 63504 which is executed on a high performance compute cluster with 268 worker nodes, 17152 Xeon Gold 6238R CPU cores and 931 TB of parallel storage.

4.2 Approximation of Neural Scaling Laws

The NSLs are fitted semi-automatically. We first manually construct a rough approximation of the NSLs by specifying a piecewise affine function at

Pseudo code 1 Experimental setup

```
1: for  $A \in \{\text{unstructured (3a), input-affine (3b), pH (3c)}\}$  do
2:   for  $S \in \{\text{spring (10), ball (11), motor (12)}\}$  do
3:     for seed  $\in \{0, \dots, N\}$  do Set seed
4:       for  $n_e \in \{1, 2, 4, \dots, 2^{14}\}$  do
5:         for  $\tilde{d} \in \{2, 4, \dots, 2^9\}$  do
6:           for  $\tilde{n}_h \in \{2, 4, 8, 16\}$  do
7:             for  $\tilde{n}_d \in \{2, 4\}$  do
8:               Sample float  $d \sim \{\tilde{d}/2, \dots, \tilde{d}\}$ ,  $n_t = \frac{1}{10}d$ 
9:               Sample integer  $n_h \sim \{\tilde{n}_h/3, \dots, \tilde{n}_h\}$ 
10:              Sample integer  $n_d \sim \{\tilde{n}_d/2, \dots, \tilde{n}_d\}$ 
11:              nMAE, nMSE,  $p = \text{main}(n_e, n_t, n_d, n_h, A, S)$ 
12:               $c = p \cdot n_e \cdot n_t \cdot 1000$ 
13:              Log (nMAE, nMSE,  $c, p, d, A, S$ )
14:            end for
15:          end for
16:        end for
17:      end for
18:    end for
19:  end for
20: end for
```

log – log scale and then automatically fit the NSLs starting with this approximation. We find that this initial guess is necessary since the problem of fitting NSLs is non-convex. To fit the NSLs, we use gradient optimization in PyTorch [16]. More precisely, we parameterize a module with parameters representing the values $\log \alpha, \log \beta, \delta, \log \sigma_i, \varphi_i, \delta_i$ for $i = 1, \dots, b$ in the representation (8). The value φ_i is capped to be higher than 0.2 by replacing it with $\max(\varphi_i, 0.2)$ whenever the module is called. This ensures numerical stability during fitting. We point out that learning $\log \beta, \log \sigma_i$ instead of β, σ_i is necessary since the latter are expected to have a high order of magnitude. It would otherwise not be possible to successfully complete the fitting, because gradient steps are typically very small.

Assume that the lower envelope E , the interpolation points $\tilde{r}_1, \dots, \tilde{r}_K$, and the evaluation of E on those points $\tilde{e}_1, \dots, \tilde{e}_K$ are given as in Definition 3.1 and we choose the number of interpolation points $K = 100$ for the fitting of all sets of outcomes. The *ADAM* optimizer [11] is used to train the

module for a few thousand iterations, in which the whole dataset is passed at each iteration. The loss function being minimized is the margin M as in (9).

5 Verification of NSLs in nonlinear system identification

In this section, we show that several types of NSLs can be observed in the context of learning-based system identification. We show that different identification methods yield reproducible NSLs across a variety of system types and prior physical knowledge levels. An overview of all the experiments and approximated NSLs is presented in the Appendix. In the following subsections, we take a closer look at a few figures that represent the general trends we noticed by inspecting all the results of the different experiments.

5.1 Compute neural scaling laws

In this section, we consider the compute NSL by considering the total amount of compute c in terms of flops used to train the model. Since the other parameters (data size and model size) influence the compute NSL, these parameters need to be varied simultaneously. Figure 1 shows the compute-nMAE NSL for the input-affine architecture on the ball system. The x -axis represents the compute in flops used to train the model (resource being scaled) and the y -axis represents the error (measured as nMAE). Individual experiments are represented by points in the plot. The point color indicates the number of trajectories used to train the model (dataset size) whereas the point size represents the model size (in terms of total parameters). The approximate NSL given by (8) determined as described in the beginning of Section 4 is represented by the blue curve. It is given by the formula

$$L(c) = .74c^{-0.039} \left[1 + \left(\frac{c}{1.2 \cdot 10^6} \right)^{\frac{1}{2}} \right]^{-1.1 \cdot 0.2} \left[1 + \left(\frac{c}{3.8 \cdot 10^6} \right)^{\frac{1}{2}} \right]^{.71 \cdot 2}.$$

We can see that the performance of models does not increase with more compute until the plateau of random guessing is being overcome at roughly 10^6 flops. The curve then follows a small segment with steep slope. It then enters a large segment where it decays linearly on log-log scale (which means

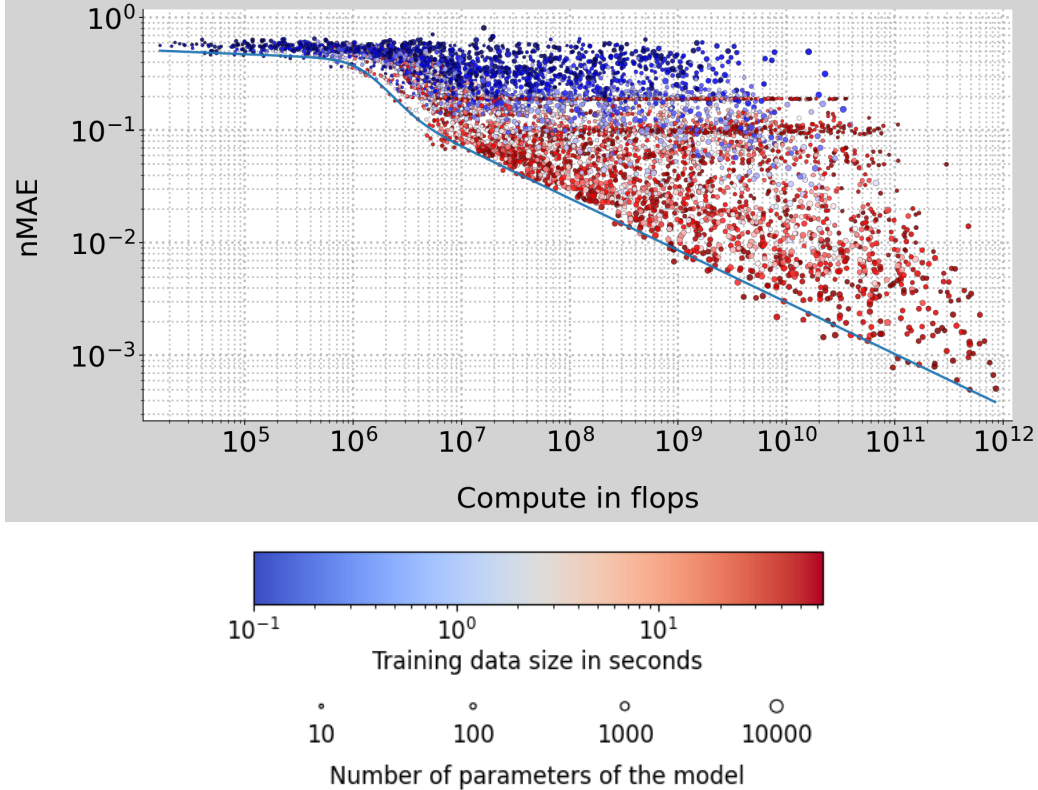


Figure 1: Compute-nMAE NSL for the input-affine architecture on data generated from the ball system

that it approximately satisfies a power law) until approximately 10^{12} flops which is the highest compute budget we considered. Hence, the NSL shown in Figure 1 has $b = 2$ breaks.

We note that within the range of 10^7 flops up to approximately 10^{12} flops, there is highly predictable scaling with the given amount of data and model parameters that we consider. We can see that the smallest points in the plot lie far away from the envelope, which shows that models need to have a minimum amount of parameters to yield compute-optimal performance. We can also see that it is necessary to have a minimum amount of data available to obtain scaling, which is indicated by points with low errors typically having a stronger red tone. Moreover, it is interesting to note that the point corresponding to the highest compute being used lies close to the envelope. This demonstrates that training models for as much as the unex-

pectedly high number $n_e = 10^{14}$ of total epochs can be necessary to obtain optimal performance. By inspecting the overview in Figure 6, we can see that the compute-nMAE NSL look very similar for all architectures and datasets we consider. This indicates that the compute necessary to obtain a certain nMAE-value is highly predictable.

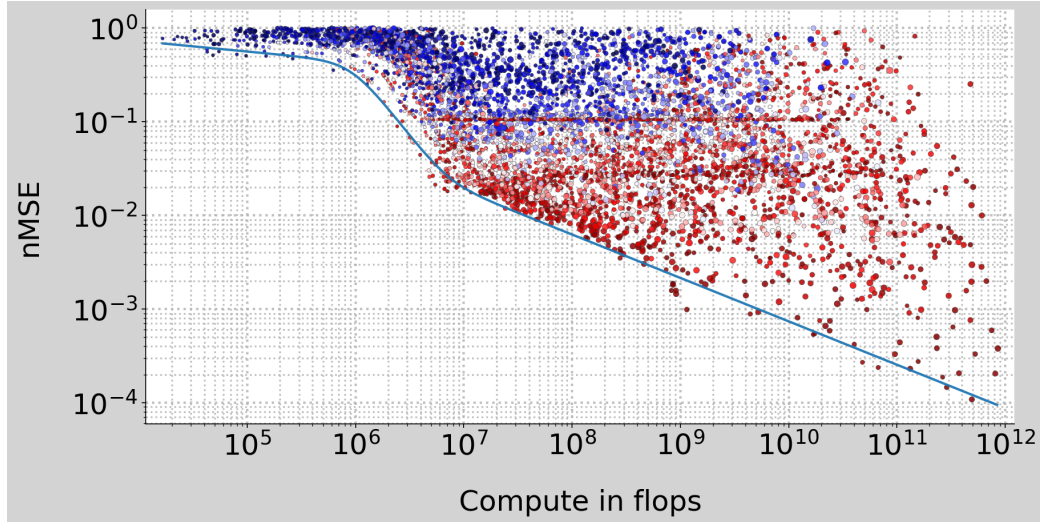


Figure 2: Compute-nMSE NSL for the input-affine architecture on data generated from the ball system.

Figure 2 shows the corresponding compute-nMSE NSL for the input-affine architecture on the motor system. The x -axis again represents the compute in flops used to train the model and the y -axis represents the error (measured as nMSE or nMAE). The NSL in Figure 2 is given by the formula

$$L(c) = 2c^{-0.11} \left[1 + \left(\frac{c}{9.3 \cdot 10^5} \right)^{\frac{1}{0.2}} \right]^{-0.28} \left[1 + \left(\frac{c}{7.1 \cdot 10^6} \right)^{\frac{1}{0.2}} \right]^{0.2}.$$

We observe $b = 2$ breaks at similar compute budgets for both error measures. We note, however, that at more than 10^{10} flops there are fewer points close to the envelope for nMSE. Inspecting the overview in Figures 6 and 7, one observes, in fact, that the nMAE NSLs tend to have fewer outliers and that there are more points located at the envelope. This suggests that nMAE could be a more suitable metric than nMSE in the context of compute NSLs.

We conclude that compute NSLs allow to predict the amount of compute (in flops) needed to obtain a certain accuracy within a very high range of possible configurations.

5.2 Data neural scaling laws

In this section, we consider data NSLs, which are obtained by treating the number of trajectories in the dataset as the resource being varied. Each point in the Figures 4 and 3 represents an element of the set of outcomes O for different training configurations. Here, the color of the points represents the amount of compute measured in flops and the number of model parameters is represented by the point size. The x -axis represents the total training time in seconds, obtained by summing the durations of all training trajectories.

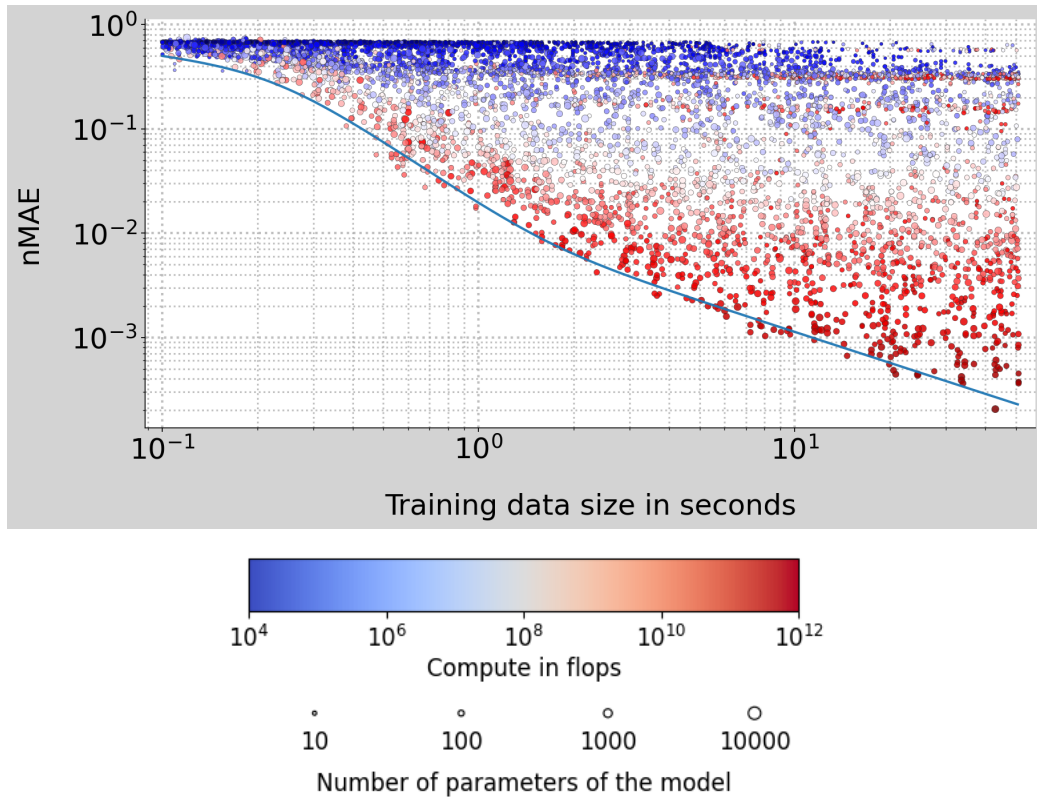


Figure 3: Data-nMAE NSL for the unstructured architecture on the motor system.

The data-nMAE NSL is shown in Figure 3 and it has $b = 2$ breaks and is given by the formula

$$L(d) = 0.22d^{-0.36} \left[1 + \left(\frac{d}{0.23} \right)^{\frac{1}{0.2}} \right]^{-0.34} \left[1 + \left(\frac{d}{1.7} \right)^{\frac{1}{0.2}} \right]^{0.22}.$$

We notice again that a minimum amount of data is necessary to overcome the plateau of random guessing which is followed by a small segment of fast progression and then ends with a long segment of smooth scaling. Similar to the compute NSL, it can be observed that the remaining two resources compute and model size play a significant role. More precisely, we observe that points close to the envelope tend to be red, especially for the higher amounts, which indicates that enough compute needs to be used to follow the data NSL. Moreover, we observe that very small points are typically not close to the envelope, which indicates that models that are too small cannot optimize the performance for a given amount of data. In addition, we observe a smooth scaling approximately from $d = 8$ s to $d = 64$ s, which indicates that the amount of data necessary to observe the desired performance can be predicted considering experiments with smaller amounts of data in this regime. Since the NSL perfectly mimics the envelope, these predictions can be considered to have a high confidence.

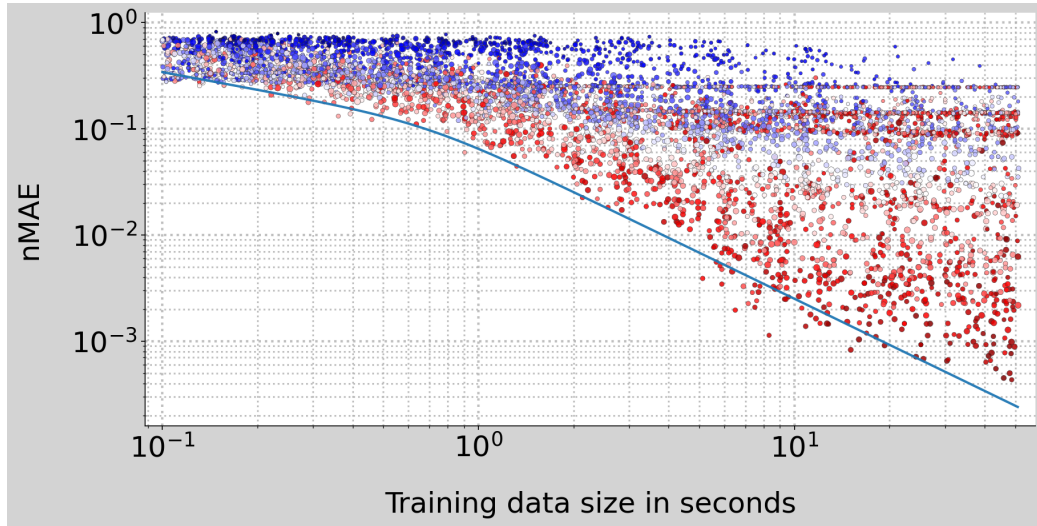


Figure 4: Data-nMAE NSL for the input-affine architecture on the spring system.

Similar behavior can be noticed in Figure 4 that shows the data-nMAE NSL for the input-affine architecture on the spring dataset which is given by the formula

$$L(d) = 0.096 d^{-0.55} \left[1 + \left(\frac{d}{0.69} \right)^{\frac{1}{0.2}} \right]^{-0.89 \cdot 0.2}.$$

However, compared to Figure 3, we can see that there are relatively many outliers at around $d = 10$ s. This means that the NSL becomes ambiguous since it is not immediately clear whether these outliers actually represent a break in the NSL. Hence the performance for $d \geq 32$ s is difficult to predict from experiments with less data, which contrasts with the observations made for the compute NSLs in Section 5.1 and the observations made for the unstructured architecture applied to the motor system shown in Figure 3. By inspecting Figures 8 and 9, we can moreover see that data NSLs look very similar for the different identification architectures considered given a fixed dataset which means that they generalize well. We also point out that the structured port-Hamiltonian architecture performs as good, even better in the case of the motor system, than the two less structured architectures considered; see Figures 8 and 9.

We conclude that data NSLs can be used to predict the error of a model at a given amount of data. However, these data NSLs can suffer from the issue that it is not always clear whether points with relatively high performance should be considered as outliers or whether they actually represent an extra break in the NSL. This phenomenon can also be seen in Figures 8 and 9, for example for the nMSE-metric on the ball system.

5.3 Model neural scaling laws

In this section, we consider model NSL which are obtained by treating the number of parameters p of the model as the resource being varied.

Figure 5 shows the model NSL for the pH architecture for the ball system. Here, the x -axis represents the number of parameters of the model. The point size indicates the dataset size and the color represents the total compute used to train the model. This NSL can be well represented using an approximation with a single break and is given by the formula

$$L(p) = 0.0003 + 0.13p^{0.22} \left[1 + \left(\frac{p}{74} \right)^{\frac{1}{0.2}} \right]^{-3 \cdot 0.2}.$$

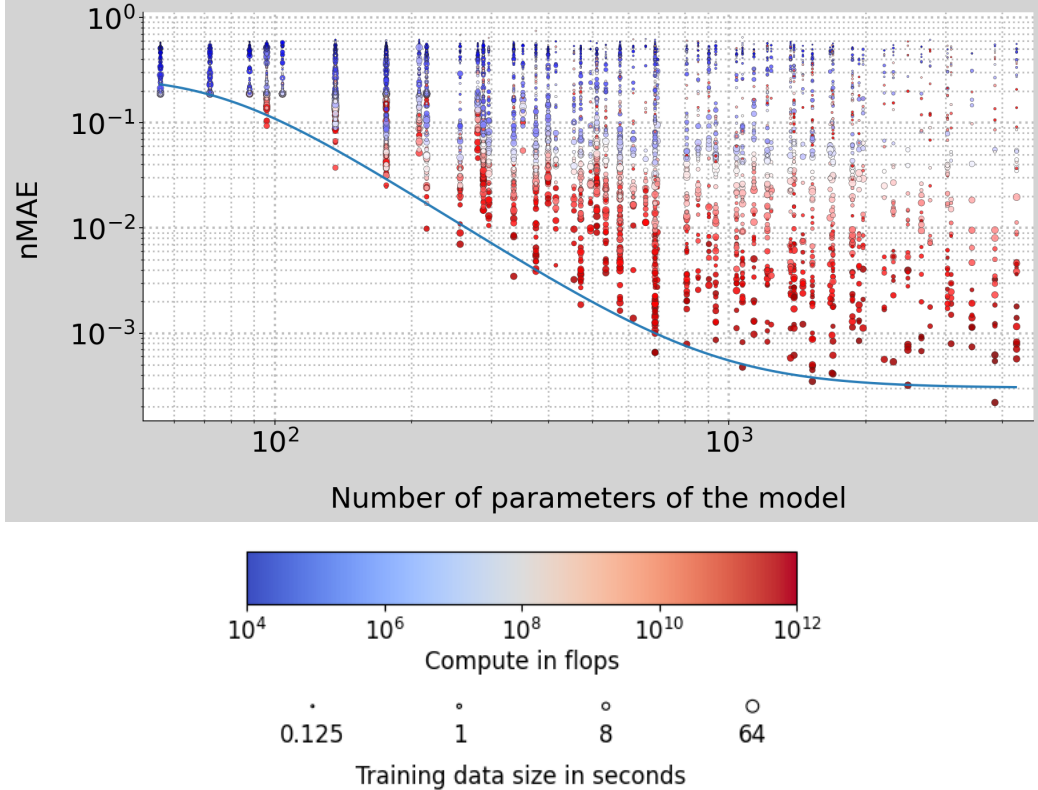


Figure 5: Model-nMAE NSL for the port-Hamiltonian architecture on the ball system.

We can see that scaling the model further than approximately 10^3 parameters does not yield better results. Note that modern hardware is often able to execute the training and inference calls of a model with 10^4 parameters with approximately the same speed as of a model with 10^3 parameters. Since this is also the case for our configuration, we infer that scaling the model parameter size is not the major bottleneck. However, it is important to note that models which are too small do not achieve optimal performance. We can also see that runs with insufficient compute or insufficient data do not achieve optimal performance at a given model size. This is not surprising since we have also observed in Sections 5.1 and 5.2 that all three resources are important to consider if one wants to optimize the performance for a given resource.

We conclude that the model size needed to obtain a given error can be

determined using NSL. We also noticed that scaling up the model was not a computational challenge in our experiments. However, it is important to scale the number of parameters of the model together with data and compute to obtain optimal results, see Figure 6.

6 Conclusion

Neural Scaling Laws (NSLs) quantify the dependence between accuracy, dataset size, model complexity, and compute available. Here, we show that NSLs can also be verified in the context of learning-based system identification for various examples and system architectures. Early trends in the scaling curve allow us to anticipate the data, compute and model complexity required for higher accuracy.

Furthermore, we observed that in system identification, the amount of data is more important than model size, which is in contrast to the results in the natural language processing community. This means that a larger model does not necessarily yield better results, as indicated by the model NSLs that are often saturating with relatively few parameters. Moreover, system models need to be trained for a very large number of iterations since training for as much as $n_e = 2^{14}$ epochs still yields improvements in the performance of the identified system model for different datasets, dataset sizes, system architectures, and model sizes.

Acknowledgment

This work was funded by the Deutsche Forschungsgemeinschaft (DFG, German Research Foundation) – Project-ID 531152215 – CRC 1701 and by the programme “Forschungsimpulse und – support (FORIS)” of the University of Wuppertal in 2024.

References

- [1] Ibrahim M Alabdulmohsin, Behnam Neyshabur, and Xiaohua Zhai. Revisiting neural scaling laws in language and vision. *Advances in Neural Information Processing Systems*, 35:22300–22312, 2022.

- [2] Yasaman Bahri, Ethan Dyer, Jared Kaplan, Jaehoon Lee, and Utkarsh Sharma. Explaining neural scaling laws. *Proceedings of the National Academy of Sciences*, 121(27):e2311878121, 2024.
- [3] Thomas Beckers, Jacob Seidman, Paris Perdikaris, and George J Pappas. Gaussian process port-Hamiltonian systems: Bayesian learning with physics prior. In *2022 IEEE 61st Conference on Decision and Control (CDC)*, pages 1447–1453. IEEE, 2022.
- [4] Blake Bordelon, Alexander Atanasov, and Cengiz Pehlevan. How feature learning can improve neural scaling laws. *J. Stat. Mech. Theory Exp.*, 2025(8):084002, 2025.
- [5] Tom Brown, Benjamin Mann, Nick Ryder, Melanie Subbiah, Jared D Kaplan, Prafulla Dhariwal, Arvind Neelakantan, Pranav Shyam, Girish Sastry, Amanda Askell, et al. Language models are few-shot learners. *Advances in Neural Information Processing Systems*, 33:1877–1901, 2020.
- [6] Ethan Caballero, Kshitij Gupta, Irina Rish, and David Krueger. Broken neural scaling laws. *arXiv:2210.14891*, 2022.
- [7] Karim Cherifi, Achraf El Messaoudi, Hannes Gernandt, and Marco Roschkowski. Nonlinear port-Hamiltonian system identification from input-state-output data. *arXiv:2501.06118*, 2025.
- [8] Mehdi Cherti, Romain Beaumont, Ross Wightman, Mitchell Wortsman, Gabriel Ilharco, Cade Gordon, Christoph Schuhmann, Ludwig Schmidt, and Jenia Jitsev. Reproducible scaling laws for contrastive language-image learning. In *Proceedings of the IEEE/CVF conference on computer vision and pattern recognition*, pages 2818–2829, 2023.
- [9] Joel Hestness, Sharan Narang, Newsha Ardalani, Gregory Diamos, Hee-woo Jun, Hassan Kianinejad, Md Mostofa Ali Patwary, Yang Yang, and Yanqi Zhou. Deep learning scaling is predictable, empirically. *arXiv:1712.00409*, 2017.
- [10] Jared Kaplan, Sam McCandlish, Tom Henighan, Tom B Brown, Benjamin Chess, Rewon Child, Scott Gray, Alec Radford, Jeffrey Wu, and Dario Amodei. Scaling laws for neural language models. *arXiv preprint arXiv:2001.08361*, 2020.

- [11] Diederik P. Kingma and Jimmy Ba. Adam: A method for stochastic optimization. *arXiv:1412.6980*, 2017.
- [12] L. Ljung. *System Identification. Theory for the user*. Prentice Hall, Upper Saddle River, USA, 2nd edition, 1999.
- [13] Alexander Maloney, Daniel A Roberts, and James Sully. A solvable model of neural scaling laws. *arXiv preprint arXiv:2210.16859*, 2022.
- [14] C. Neary and U. Topcu. Compositional learning of dynamical system models using port-Hamiltonian neural networks. In *Proceedings of Machine Learning Research vol 211:1–17, 2023 5th Annual Conference on Learning for Dynamics and Control*, 2023.
- [15] Elliot Paquette, Courtney Paquette, Lechao Xiao, and Jeffrey Pennington. 4+3 phases of compute-optimal neural scaling laws. *Advances in Neural Information Processing Systems*, 37:16459–16537, 2024.
- [16] Adam Paszke, Sam Gross, Francisco Massa, Adam Lerer, James Bradbury, Gregory Chanan, Trevor Killeen, Zeming Lin, Natalia Gimelshein, Luca Antiga, Alban Desmaison, , et al. PyTorch: An imperative style, high-performance deep learning library. In *Advances in Neural Information Processing Systems 32*, pages 8024–8035. Curran Associates, Inc., 2019.
- [17] Mario Spirito, Yann Le Gorrec, and Bernhard Maschke. Structure-preserving observers for port-Hamiltonian systems via contraction analysis. *hal-04344593v2*, 2024.
- [18] A. J. van der Schaft and D. Jeltsema. Port-Hamiltonian Systems Theory: An Introductory Overview. *Found. Trends Systems Control*, 1(2-3):173–378, 2014.
- [19] G. J. E. van Otterdijk, S. Moradi, S. Weiland, R. Tóth, N. O. Jaensson, and M. Schoukens. Learning subsystem dynamics in nonlinear systems via port-Hamiltonian neural networks. *arXiv:2411.05730*, 2024.
- [20] Ngoc Minh Trang Vu, Thanh Hung Pham, Ionela Prodan, and Laurent Lefèvre. Port-Hamiltonian observer for state-feedback control design. In *2023 European Control Conference (ECC)*, pages 1–6. IEEE, 2023.

- [21] Matei Zaharia, Andrew Chen, Aaron Davidson, Ali Ghodsi, Sue Ann Hong, Andy Konwinski, Siddharth Murching, Tomas Nykodym, Paul Ogilvie, Mani Parkhe, et al. Accelerating the machine learning lifecycle with mlflow. *IEEE Data Eng. Bull.*, 41(4):39–45, 2018.
- [22] Xiaohua Zhai, Alexander Kolesnikov, Neil Houlsby, and Lucas Beyer. Scaling vision transformers. In *Proceedings of the IEEE/CVF conference on computer vision and pattern recognition*, pages 12104–12113, 2022.

A Example systems

We use the same examples as in [7].

A.1 Spring system

We consider the interconnection of two nonlinearly damped mass-spring systems with

$$H(x) = \sum_{i=1}^2 \frac{k_i q_i^2}{2} + \frac{p_i^2}{2m_i}, \quad B(x) = \begin{bmatrix} 0 & 1 & 0 & 0 \\ 0 & 0 & 0 & 1 \end{bmatrix}^\top, \quad (10)$$

$$J(x) = \begin{bmatrix} 0 & 1 & 0 & 0 \\ -1 & 0 & 1 & 0 \\ 0 & -1 & 0 & 1 \\ 0 & 0 & -1 & 0 \end{bmatrix}, \quad R(x) = \begin{bmatrix} 0 & 0 & 0 & 0 \\ 0 & \frac{b_1 p_1^2}{m_1^2} & 0 & 0 \\ 0 & 0 & 0 & 0 \\ 0 & 0 & 0 & \frac{b_2 p_2^2}{m_2^2} \end{bmatrix},$$

with $x = [q_1 \ p_1 \ q_2 \ p_2]^\top$. The parameter values are shown in Table 1. We will refer to this system as the *spring system*.

A.2 Ball system

The second system we consider is magnetically levitated ball system from [3], which is referred to as the *ball system*. In that case

$$H(x) = \frac{x_1^2}{2m} + \frac{1}{2} \frac{x_3^2}{L(x_1)}, \quad B(x) = [0 \ 0 \ 1]^\top, \quad (11)$$

$$J(x) = \begin{bmatrix} 0 & 1 & 0 \\ -1 & 0 & 0 \\ 0 & 0 & 0 \end{bmatrix}, \quad R(x) = \begin{bmatrix} 0 & 0 & 0 \\ 0 & c|x_2| & 0 \\ 0 & 0 & \frac{1}{R} \end{bmatrix},$$

symbol	meaning	value	unit
m_1	mass 1	1	[kg]
m_2	mass 2	1.5	[kg]
b_1, b_2	damping coefficient	2	-
k_1	spring constant 1	1	[N/m]
k_2	spring constant 2	0.1	[N/m]

Table 1: Mass spring system parameters

where $x = [x_1 \ x_2 \ x_3]^\top$ with x_1 representing the vertical position of the ball, x_2 its momentum and x_3 the magnetic flux. The parameter values are

symbol	meaning	value	unit
m	ball mass	0.1	[kg]
$L(x_1)$	inductivity at height x_1	$(0.1 + x_1^2)^{-1}$	[H]
R	electrical resistance	0.1	[Ω]
c	drag coefficient	1	-

Table 2: Iron ball system parameters

shown in Table 2.

A.3 Motor system

The third system we consider is the permanent synchronous motor, see [20, 17], which is referred to as the *motor system*.

The system structure is

$$H(x) = \frac{\varphi_d^2}{2L} + \frac{\varphi_q^2}{2L} + \frac{p^2}{2J_m}, \quad B = \begin{bmatrix} 1 & 0 & 0 \\ 0 & 1 & 0 \end{bmatrix}^\top \quad (12)$$

$$J(x) = \begin{bmatrix} 0 & 0 & \varphi_q \\ 0 & 0 & -\varphi_d - \Phi \\ -\varphi_q & \varphi_d + \Phi & 0 \end{bmatrix}, \quad R(x) = \begin{bmatrix} r & 0 & 0 \\ 0 & r & 0 \\ 0 & 0 & \beta \end{bmatrix},$$

with $x = [\varphi_d \ \varphi_q \ p]^\top$, φ_d and φ_q are magnetic fluxes while p is the rotor momentum.

symbol	meaning	value	unit
J_m	inertia	0.012	$[\text{kg} \cdot \text{m}^2]$
L	phase inductance	$3.8 \cdot 10^{-3}$	[H]
β	viscous friction coefficient	0.0026	[Nms/rad]
r	phase resistance	0.225	$[\Omega]$
Φ	constant rotor magnetic flux	0.17	[Wb]

Table 3: Permanent synchronous motor system parameters

The parameter values are shown in Table 3.

B Overview of NSLs

In this section, we collect the figures of all considered NSLs. The compute-nMAE NSLs are shown in Figure 6. All compute-nMSE NSLs are shown in Figure 7. The data-nMAE NSLs are shown in Figure 8. All data-nMSE NSLs are shown in Figure 9. The model-nMAE NSLs are shown in Figure 10. All model-nMSE NSLs are shown in Figure 11.

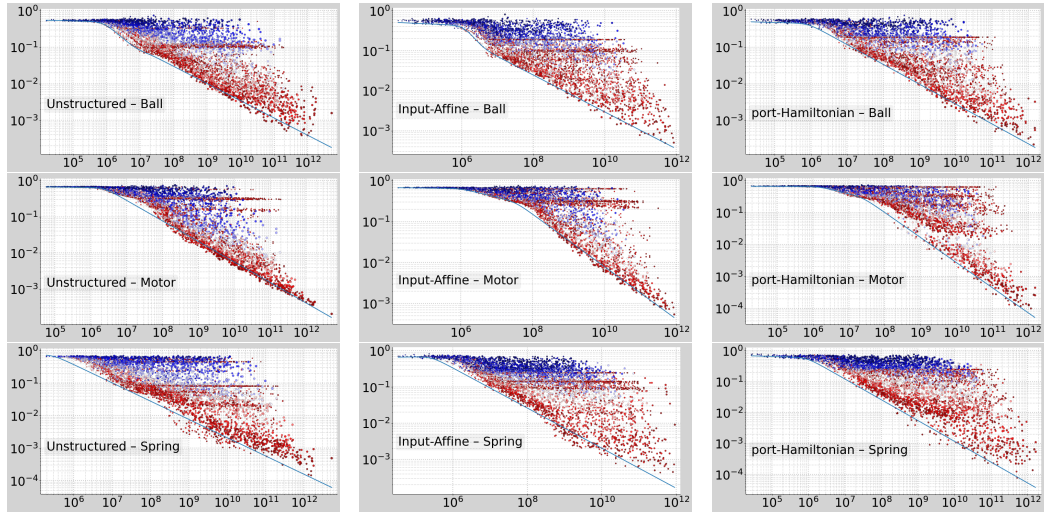


Figure 6: All compute-nMAE NSLs

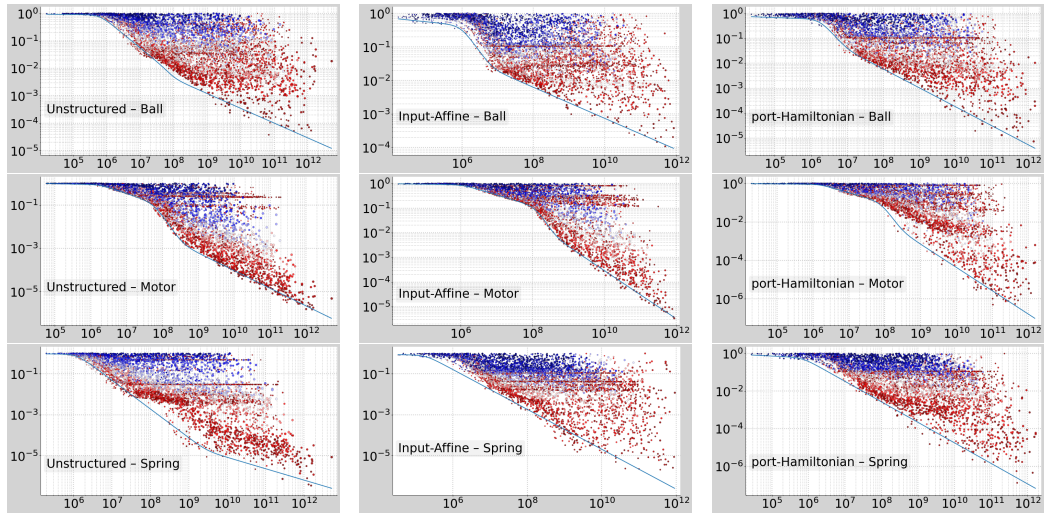


Figure 7: All compute- nMSE NSLs

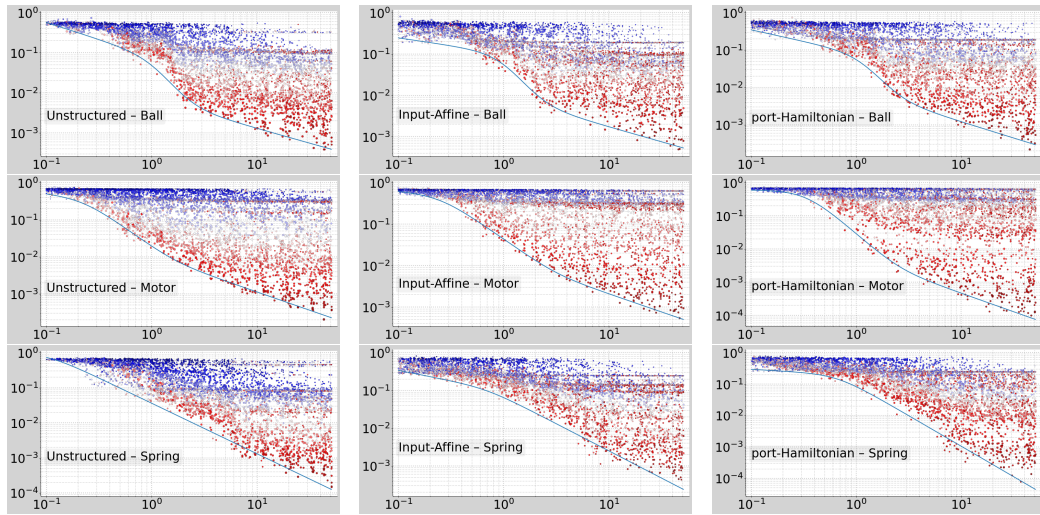


Figure 8: All data-nMAE NSLs

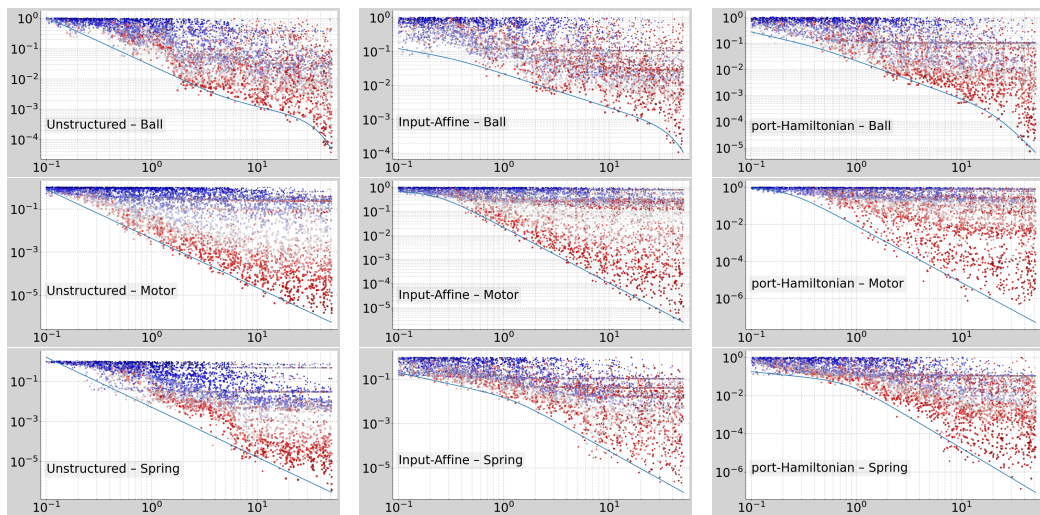


Figure 9: All data-nMSE NSLs

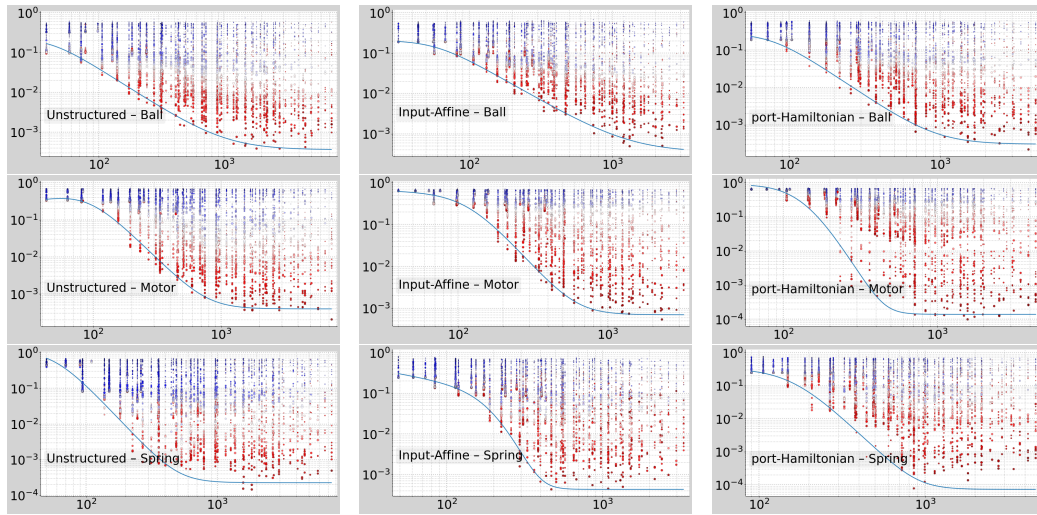


Figure 10: All model-nMAE NSLs

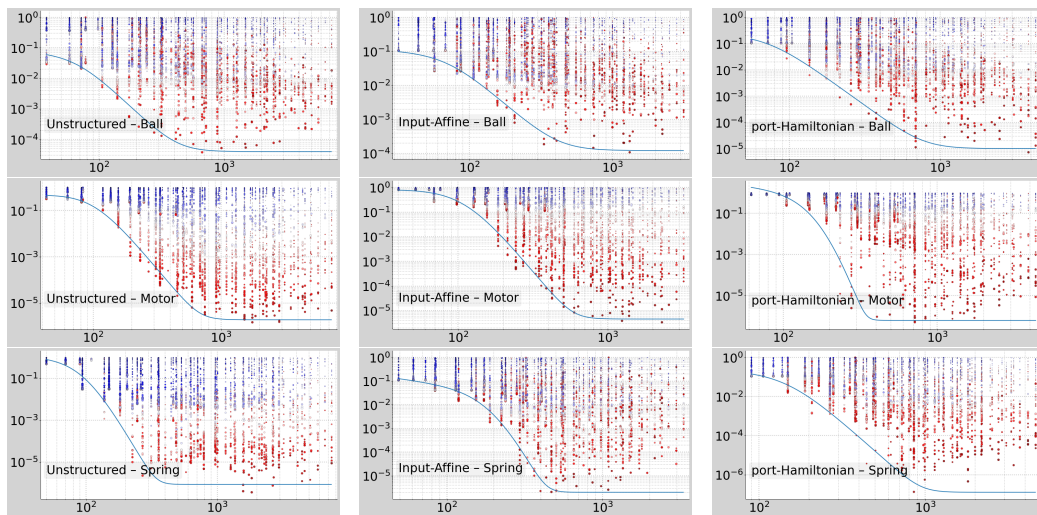


Figure 11: All model-nMSE NSLs